Article

The Relationship between Bacterial Sulfur Cycling and Ca/Mg Carbonate Precipitation—Old Tales and New Insights from Lagoa Vermelha and Brejo do Espinho, Brazil

Vanessa Fichtner [1,*], Simon L. Schurr [2], Harald Strauss [2], Crisógono Vasconcelos [3], Katja E. Goetschl [4], Camila Areias [5,6], Catia F. Barbosa [5] and Adrian Immenhauser [7,8]

1 Department of Biology and Environmental Science, Linnæus University, 39182 Kalmar, Sweden
2 Institut für Geologie und Paläontologie, Westfälische-Wilhelms-Universität Münster, Corrensstraße 24, 48149 Münster, Germany
3 Centro de Desenvolvimento Tecnológico, Núcleo de Inovação e Tecnologia do Serviço Geológico do Brasil, Rio de Janeiro 22290-180, Brazil
4 Institute of Applied Geosciences, Graz University of Technology, Rechbauerstrasse 12, 8010 Graz, Austria
5 Departamento de Geoquímica, Universidade Federal Fluminense, Niterói 24020-141, Brazil; c.areiasdeoliveira@vu.nl (C.A.); catiafb@id.uff.br (C.F.B.)
6 Department of Earth Sciences, Vrije Universiteit Amsterdam, 1081 HV Amsterdam, The Netherlands
7 Institute of Geology, Mineralogy and Geophysics, Ruhr-University Bochum, Universitätsstraße 150, 44801 Bochum, Germany
8 Fraunhofer IEG (Institution for Energy Infrastructures and Geothermal Systems), Am Hochschulcampus 1, 44801 Bochum, Germany
* Correspondence: vanessa.fichtner@lnu.se

Abstract: Over the few past decades, the concept of microbial sulfur cycling catalyzing the precipitation of $CaMg(CO_3)_2$ at low temperatures ($<40\,^\circ C$) has been studied intensely. In this respect, two hypersaline lagoons, Lagoa Vermelha and Brejo do Espinho, in Brazil, have been the subject of numerous studies investigating sedimentary Ca/Mg carbonate formation. Here, we present the sulfur and oxygen isotopic compositions of dissolved sulfate from surface water, as well as sulfate and sulfide from pore-water ($\delta^{34}S_{SO4}$, $\delta^{18}O_{SO4}$, and $\delta^{34}S_{H2S}$), the sulfur isotopic composition of sedimentary pyrite ($\delta^{34}S_{CRS}$), and sulfur and oxygen isotopic compositions of carbonate-associated sulfate (CAS, $\delta^{34}S_{CAS}$ and $\delta^{18}O_{CAS}$). The pore-water profiles at Lagoa Vermelha indicate ongoing bacterial sulfate reduction by increasing $\delta^{34}S_{SO4}$, $\delta^{18}O_{SO4}$ and $\delta^{34}S_{CRS}$ values downcore. At Brejo do Espinho, the pore-water profiles displayed no depth-dependent isotope trends; the Ca/Mg ratio was, on average, lower, and the $\delta^{18}O_{SO4}$ values in both surface and pore-water were strongly enriched in ^{18}O. There was an overall mismatch between $\delta^{34}S_{SO4}$ and the significantly higher $\delta^{34}S_{CAS}$ values. A negative correlation was observed between the Ca/Mg ratio and higher $\delta^{34}S_{CAS}$ values. The results show that the size difference between the two lagoons induces differences in the intensity of evaporation, which leads to the increased secretion of extrapolymeric substances (EPSs) by microbes in the smaller Brejo do Espinho. EPS provides the microenvironment where Ca/Mg carbonate can nucleate and preserve increased $\delta^{34}S_{CAS}$ values. Apart from EPS, increased sulfur oxidation is proposed to be a second factor causing relative enrichment of Ca/Mg carbonates at Brejo do Espinho. Our results emphasize the role of evaporative processes on Ca/Mg carbonate formation, and indicate that the respective $\delta^{34}S_{CAS}$ values reflect microenvironments rather than preserving an open marine $\delta^{34}S_{SO4}$ signature.

Keywords: sulfur cycling; carbonate-associated sulfate; sedimentary dolomite; Lagoa Vermelha; Ca/Mg carbonate formation

1. Introduction

Carbonates are perhaps the most important archives for reconstructing the evolution of the complex marine and global biogeochemical processes that shaped modern Earth [1,2].

Among this large group of sediment rocks, dolomite (and intermediate phases between calcite and dolomite) comprises a group of carbonates with varying Ca/Mg ratios and crystal lattice structures [2]. Early diagenetic replacement dolomite builds up massive Precambrian and Paleozoic carbonate platforms [1–5]. In younger sedimentary rocks, however, the volumes of dolomite and related Mg/Ca minerals continuously decrease relative to calcite and aragonite [6–8]. In the Holocene, dolomite is scarce and mostly occurs as calcian dolomite or even as metastable very-high-Mg calcite, i.e., minerals that share similarities with dolomite in terms of their geochemistry, but still have crystal structures similar to that of calcite [2,9–11]. Acknowledging the variety of carbonate minerals and their transition between Mg calcite, very-high-Mg calcite, and calcian dolomite, the descriptive label 'Ca/Mg carbonate' is used in this study as an umbrella term.

Due to the scarcity of Ca/Mg carbonate in the Neogene sedimentary rock record, many studies have investigated the conditions required for dolomite formation and stabilization in modern environments (please refer to reviews by [2,11,12]). Hypersaline conditions combined with bacterial activity—and especially that of sulfate-reducing microbes—have emerged as one critical factor in promoting sedimentary Ca/Mg carbonate formation [12–22]. Bacterial sulfate reduction (BSR) increases pore-water alkalinity, the saturation state of dolomite in extracellular polymeric substances (EPSs), and it can overcome the hydration barrier of Mg^{2+} ions [11,19,23–26]. Moreover, BSR reduces the sulfate concentration, which some have considered to inhibit dolomite precipitation [27,28]. BSR produces hydrogen sulfide, which also promotes dolomite formation [26]. In contrast, [12] proposed that the metabolism of sulfate-reducing bacteria (SRB) acts as a catalyst for dolomite precipitation processes in microenvironments. Sulfate ions form strong ionic pairs with Mg ions in seawater. During bacterial sulfate reduction, sulfate ions are consumed, releasing Mg and bicarbonate ions. Thus, the conditions to overcome the kinetic barrier to dolomite nucleation can be achieved.

The coastal lagoons Lagoa Vermelha and Brejo do Espinho are two of the few locations worldwide where syngenetic Ca/Mg carbonate forms under near-surface conditions [12]. Recently, Ref. [22] provided XRD data documenting the existence of calcian and well-ordered dolomite in those lagoons. The Lagoa Vermelha and Brejo do Espinho are characterized by hypersaline conditions and a vital microbial community forming layered mats on the lagoonal surfaces [12,21,29]. Within the limitations of an approach that compares the Phanerozoic with the Precambrian world, Lagoa Vermelha and its unique biogeochemical conditions have been considered a Precambrian 'analogue' [17]. Prior studies have compared the activity of sulfur-metabolizing bacteria in both lagoons and observed differences in the sulfur isotope composition of the pore-waters and the distribution of Ca/Mg carbonate horizons in the sediment columns [16,29]. To draw connections and conclusions to early marine diagenetic dolomite formation in the geological past, however, it is insufficient to analyze the sulfur phases in the pore-water of modern lagoons. Moreover, it is critical to understand the type of information encoded in a specific geochemical proxy—here, carbonate-associated sulfate (CAS)—relevant for the reconstructions of diagenetic environments triggering Ca/Mg carbonate precipitation in aquatic environments.

Carbonate-associated sulfate (CAS) is substituted in the carbonate crystal lattice and (within a 1‰ range; see [30]) is considered to reflect the $\delta^{34}S$ value of dissolved sulfate of ambient water from which the carbonate precipitates. CAS has been used as a proxy for reconstructing the marine $\delta^{34}S_{SO4}$ value from the Phanerozoic [31,32]. The CAS sulfur isotope values best represent the upper water signature, where BSR is limited, the TOC is low, and the carbonate crystal is stable before sulfate from microbially evolved pore-water can be incorporated [33]. In contrast, both lagoons are characterized by active BSR in a TOC-rich sediment [12,16,21,29]. Thus, the $\delta^{34}S_{CAS}$ values for both lagoons will likely reveal more about the processes in the pore-water than reflect the sulfate in the surface water.
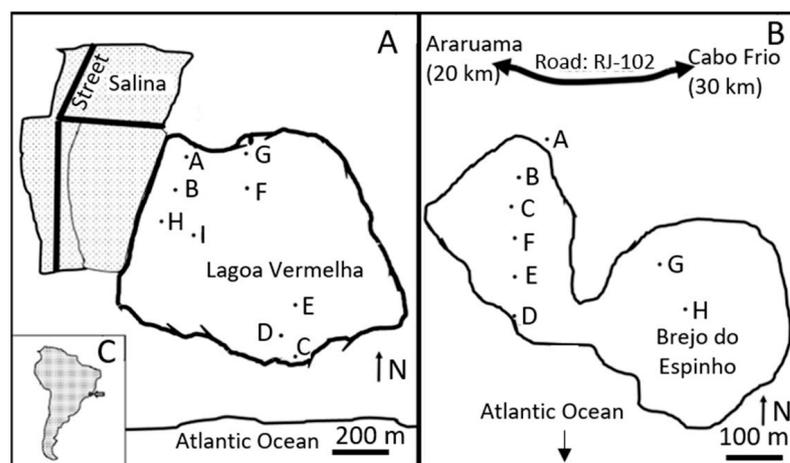
Therefore, the primary goal of the present study was to understand the CAS signatures in Lagoa Vermelha and Brejo do Espinho, and establish the characteristic CAS values for these unique environments. In addition, this study assesses whether the sulfur isotope

signals of different sulfur phases yield relevant information about the mechanism of Ca/Mg carbonate formation in near-seafloor environments. For this, the sulfur and oxygen isotope compositions of dissolved sulfate and sulfide in the surface water and the pore-water, as well as from pyrite and CAS in the sediment of multiple cores from both lagoons, were analyzed. That way, the sulfur cycling in both Lagoa Vermelha and Brejo do Espinho could be characterized, and the CAS signals preserved in the carbonate sediments were set in the context of Ca/Mg carbonate precipitation. These data show that $\delta^{34}S_{CAS}$ signals in sedimentary Ca/Mg carbonates might not be used as seawater proxies, but rather as proxies for formation conditions, which is of great significance for carbonate archive research beyond the case example documented here.

2. Study Area

The two lagoons, Lagoa Vermelha (S 22°55′33.7″; W 42°22′12.9″) and Brejo do Espinho (S 22°56′1.2″; W 42°22′20.7″), are located 120 km east of Rio de Janeiro (Brazil), close to Cabo Frio. Both lagoons are situated between two Holocene sand banks on the shoreline of the Atlantic Ocean (Figure 1). To the north of both lagoons, the much larger and hyper-saline Araruama Lagoon is situated. The region has a semi-arid climate with wet and dry periods [34], which are influenced by an upwelling area in the Atlantic Ocean at Cabo Frio. Lagoa Vermelha has an area of 2 km², an average water depth of approximately 1 m, and a surface water temperature between 22 and 32 °C (Figure 2) [12,21,35]. Brejo do Espinho is a smaller lagoon with a surface area of 1 km² and a water depth of less than 0.5 m [16]; the surface water temperature varies between 22 and 33 °C (Figure 2) [16,21]. In Lagoa Vermelha, the sediment surface is partially composed of a 1 cm thin lithified carbonate crust. In addition, 1 m long and 0.5 m high stromatolite mounds are observed (Figure 2A). The first meter of sediment below the carbonate crust is an aphanitic layer, but also comprises laminated layers with carbonate and bivalve shells (*Anomalocardia brasiliensis*) [12,35]. High Mg-calcite and Ca-dolomite (42 up to 48 mol-% MgCO₃) constitute the main mineralogy of the sediment [12,16,35,36]. Further down, the sediment comprises marine quartz sand and wood [35]. The formation dates of both lagoons date back to 4200 years BP [18]. After the Holocene marine transgression, the sea level reached the maximum at 4500 years BP and started dropping until reaching the current level at 1500 years BP [37].

The sediment surface of Brejo do Espinho is covered with a 2 cm thin microbial mat (Figure 2D,H). Below this, Ca/Mg carbonate sediment occurs with Ca/Mg calcite and non-stoichiometric dolomite (48 mol-% MgCO₃) [16,21]. At a depth of 0.45 m is a marine quartz-rich layer with coquina, aged 1750 ± 86 years BP [16].

Figure 1. Lagoa Vermelha (**A**) and Brejo do Espinho (**B**) are close to the shoreline of the Atlantic Ocean and approximately 120 km east of Rio de Janeiro, Brazil (**C**). The letters show the locations of each drilled core (see Supplementary Materials).

Figure 2. Photos of Lagoa Vermelha and Brejo do Espinho. (**A**) Northern shoreline of Lagoa Vermelha with salty foam accumulating on the beach. View from the north-western part of the lagoon. (**B**) Northern shoreline of Brejo do Espinho close to sampling location (**B**). White salty foam has precipitated, and dry cracks have developed. (**C**) Stromatolites in Lagoa Vermelha. (**D**) Flooded dry cracks from the past few years in Brejo do Espinho. (**E**) Close-up of the typical sediment core. White thin carbonate layers and grey layers where iron sulfides have precipitated. (**F**) Seaward side of Brejo do Espinho near sampling location (**D**). View from south to north. The white sediment consists of carbonate with only small siliciclastic portions. Dark spots are small stromatolites. (**G**) Sediment core showing different colored layers representing carbonate with different levels of iron sulfides. (**H**) Microbial mat taken from Brejo do Espinho.

3. Sampling and Methodology

3.1. Sampling Strategy and Fieldwork

Lagoonal surface water, pore-water, and sediment were collected in March 2018. Push cores were sampled along landward-seaward transects (Figure 1). The focus was placed on the upper 0.4 m of the sediment column. Pore-water was extracted from the sediment core using Rhizon samplers [38] and transferred into polypropylene vials containing 2 mL of 0.16 M ammoniacal zinc acetate solution to stabilize volatile hydrogen sulfide as a solid zinc sulfide precipitate. In addition, H_2S gas bubbles directly below the microbial mat were sampled at Brejo do Espinho for 4 h via Rhizon samplers connected to a syringe filled with ammoniacal zinc acetate solution precipitating zinc sulfide. Sediment cores were sampled and described in the field. Subsequently, the sediment was freeze-dried for geochemical analysis at the University of Münster, Germany. Furthermore, portions of a stromatolithic build-up were sampled at Lagoa Vermelha. Additional lagoonal surface water samples were collected for both lagoons over an annual cycle between June 2018 and March 2019.

3.2. Sample Preparation and Laboratory Analyses

Pore-water sulfide (precipitated as solid zinc sulfide) was separated from the bulk pore-water sample via filtration using a cellulose–nitrate filter ($\leq$0.45 μm pore size) and then dried at 40 °C. Surface water samples were filtered ($\leq$0.45 μm pore size). In surface water and pore-water samples, sulfate was precipitated as barium sulfate with 0.41 M $BaCl_2$ solution under acidic conditions (pH < 2) at 80 °C for 3 h. Sulfate concentrations were determined gravimetrically.

The total organic carbon (TOC) content of the freeze-dried bulk sediment was quantified via infrared spectroscopy using a carbon-sulfur analyzer (CS-580, Eltra Elemental Analyzers) with a standard deviation of $\leq$0.8 wt.% (2 S.D.). In order to prepare the samples for geochemical analyses, freeze-dried sediments were sieved (nylon, 200 μm pore size) in order to remove all biogenic carbonates, such as bivalve and gastropod shells and lithified microbial mat components from Ca/Mg carbonates. Furthermore, bivalves and balanids were separated manually from the stromatolitic mound matrix, and a firmground specimen was sampled in the Lagoa Vermelha.

Following separation, all samples were pulverized using a tungsten carbide mill. In order to avoid contamination with skeletal carbonates during subsequent CAS extraction, powder X-ray diffraction (Philips, Almelo, the Netherlands, X'Pert powder diffractometer, CuKα, 5–55° 2θ, 0.02 °/step, 1 s/step) was applied to determine the sample mineralogy. In addition, the mineralogy of one bivalve shell from Brejo do Espinho was determined by X-ray diffraction. Approximately 2 g of the Ca/Mg carbonate fraction was purified to determine the Ca^{2+}/Mg^{2+} ratio. These samples were leached four times using deionized water for 24 h. Subsequently, samples were dissolved for 24 h at 20 °C in 3 M HNO_3, and the magnesium and calcium contents were measured via inductively coupled plasma optical emission spectrometry (ICP-OES, ThermoFisher Scientific^{TM}, Waltham, MA, USA, iCAP 6500DUO) at the Ruhr University Bochum. International certified standards BCS-CRM 512 and 513 (dolomite and calcite) were used with a long-term reproducibility of $\leq$1.0 wt.% (2 S.D.) for calcium and $\leq$0.4 wt.% (2 S.D.) for magnesium.

For CAS extraction, approximately 60 g of sediment powder (Ca/Mg carbonates or bivalve shells) was leached with 1.71 M NaCl solution for 24 h. The solution was constantly agitated with a magnetic stirrer. The NaCl leaching was repeated five times. Finally, sediment was rinsed once with deionized water to remove all water-soluble sulfate (residual freeze-dried pore-water sulfate). Subsequently, the Ca/Mg carbonate fraction was dissolved in 8 M HCl under permanent stirring. The solution was filtered (through a cellulose nitrate filter with 0.45 μm pore diameter), and 50 mL of 0.41 M $BaCl_2$ solution was added to precipitate the dissolved carbonate-associated sulfate as solid $BaSO_4$. The precipitate was filtered off and dried, and the CAS content was determined gravimetrically. The insoluble residuum was collected on filter paper further to extract sedimentary sulfide minerals (e.g., pyrite) using the chromium reduction method [39].

For the chromium reduction method, 12 g of bulk sediment, 4 g of the insoluble residual sediment (e.g., organic, sulfides) after CAS extraction, and dried zinc sulfide were weighed into digestion flasks. Based on a poor acid volatile sulfur (AVS) yield (<200 µg Ag_2S), the determination of the sulfur isotopic ratio of AVS was not possible. Subsequently, 10 mL of ethanol was added, and the reaction vessel was connected to a bulb condenser and two gas-washing flasks. The first flask was filled with deionized water, and the second flask was filled with 0.2 M zinc acetate acetic acid solution to trap the hydrogen sulfide as zinc sulfide. Furthermore, 20 mL of 8 M HCl and 30 mL of 1 M $CrCl_2$ solution were added to the sample in the digestion flasks, and sulfide was converted to H_2S (g) at 85 °C in a nitrogen atmosphere for 2 h. H_2S (g) passed through the deionized water and was precipitated as zinc sulfide in the second flask. Subsequently, ZnS (s) was converted to Ag_2S (s) by adding 10 mL of 0.1 M $AgNO_3$ solution. Finally, Ag_2S (s) was filtered off using a cellulose nitrate filter ($\leq$0.45 µm pore diameter) and dried overnight at 40 °C. The Ag_2S (s) yield was determined gravimetrically.

3.3. Isotope Analysis

For $\delta^{34}S$ isotope analysis, 400 µg of $BaSO_4$ (s) (surface water, pore-water sulfate, and CAS) or 400 µg of Ag_2S (s) (pore-water sulfide and sedimentary pyrite) was placed into tin capsules and mixed with 700 µg V_2O_5 (s) to catalyze the combustion to SO_2 (g). The sulfur isotopic composition was measured via EA-IRMS (using a Thermo Scientific Delta V Advantage isotope ratio mass spectrometer interfaced with a Flash-EA-IsoLink-CN elemental analyzer) at the University of Muenster. The long-term external reproducibility for $\delta^{34}S$ was better than 0.5‰ (2 S.D.). All samples were calibrated to the V-CDT scale with the IAEA standards S-1, S-2, S-3, and NBS-127. The analytical performance (accuracy and precision) was monitored using internal laboratory standards (Ag_2S (s) and CdS (s)).

For $\delta^{18}O$ isotope analysis, 200 µg of $BaSO_4$ (s) (surface water, pore-water sulfate, and CAS) was weighed into silver capsules and measured using a TC/EA-IRMS (high-temperature conversion elemental analyzer connected to a Thermo Scientific Delta V Plus) at the University of Muenster. The oxygen isotope ratio was calibrated using the V-SMOW scale with IAEA standards SO-5, SO-6, and NBS-127, and the analytical performance was monitored with an internal laboratory standard $BaSO_4$ (s). The external reproducibility was better than 1.0‰ (2 S.D.).

4. Results

4.1. Field Observations and Facies Description

During fieldwork at Lagoa Vermelha in March 2018, the water depth in the lagoon was up to 1 m, and surface water had a temperature of 31.8 °C, a pH-value of 8.2 and a salinity of 67 PSU. At Brejo do Espinho, the water depth was 0.2 m, the surface water temperature was 38.9 °C, the pH was 9.8, and the salinity was 80 PSU.
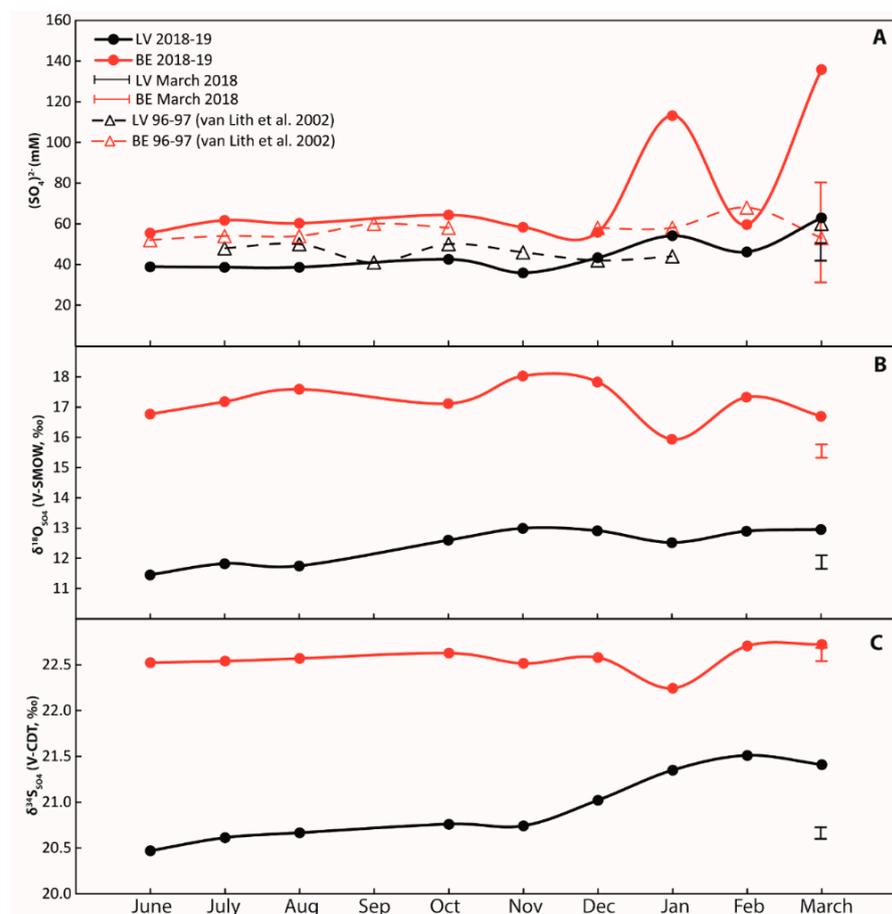
Along the shoreline of Lagoa Vermelha, a salty foam had accumulated. Within the lagoon, the surficial firmground covering parts of the lagoonal floor was overgrown with green algae. Beneath this interval was a dark, fine-grained carbonate mud containing bivalve shells. The TOC content reached a maximum of 16 wt.% (Supplementary Table S3). At a depth of 0.2 to 0.4 m beneath the lagoonal floor, finely laminated (1 mm thin), lithified carbonate crusts (Figure 2E), carbonate concretions ($\leq$3 cm), carbonate pellets, quartz sand, and bivalve shells were present. In the lowest part of the cores (>0.4 m), quartz sand with bivalve shells was found.

Similarly to Lagoa Vermelha, the shoreline of Brejo do Espinho was surrounded by salty foam. At Brejo do Espinho, dry cracks had developed, and desiccation cracks from subaerial exposure events during the past few years were visible at the lagoonal floor still covered by water (Figure 2B,D). The seaward side consisted of a white, almost pure carbonate beach with occasional small stromatolites, 2 cm in size (Figure 2F). At Brejo do Espinho, the occasional smell of ammonia and hydrogen sulfide could be noticed during field work. Laminated microbial mats with an upper green layer and a lower red
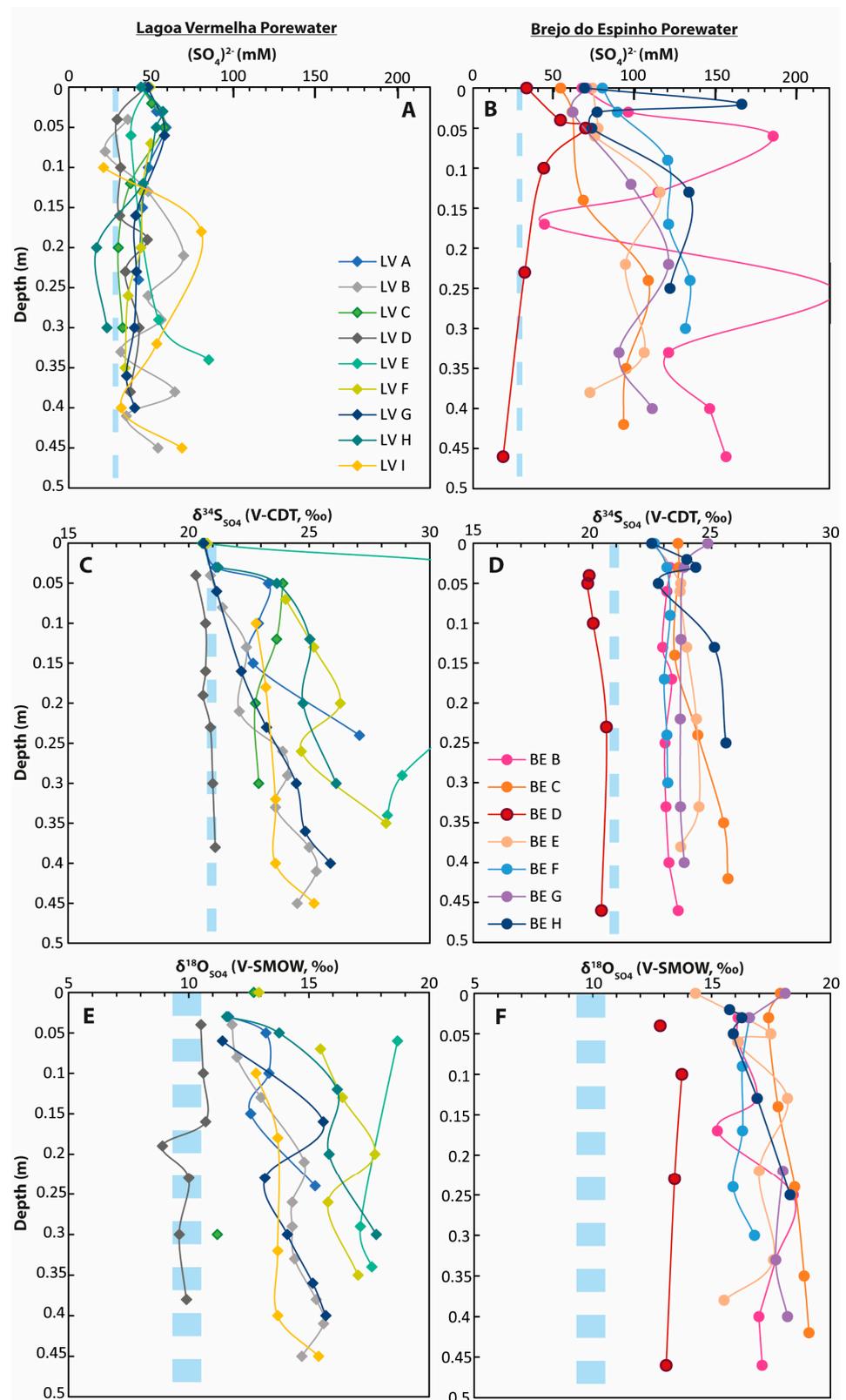
and brown layer covered the lagoonal floor in Brejo do Espinho (Figure 2H). These mats contained small (<1 mm) carbonate pellets. Between the microbial mat and the underlying carbonate sediment, gas bubbles accumulated. Further downcore, fine-grained carbonate muds were found. No evidence of bioturbation was found in the Brejo do Espinho. In the lower part of the sediment core (0.45 m depth), bivalve shells, quartz sand, and carbonate mud dominated. The upper sediment layer had a TOC content of up to 10 wt.%, but then continuously decreased to 4 wt.% at a depth of 0.45 m beneath the lagoonal floor (Supplementary Table S5).

4.2. Geochemistry of Water Samples

All results for surface and pore-water are shown in Figures 3 and 4, as well as in the Supplementary Materials. Over an annual cycle, surface water sulfate concentrations varied between dry (June to August 2018) and wet seasons (October to March 2019). Sulfate concentrations at Lagoa Vermelha ranged from 36 to 63 mM, and at Brejo do Espinho from 56 to 136 mM, respectively (Figure 3A, Supplementary Table S1). Sulfur isotope data for surface water sulfate at Lagoa Vermelha lie between 20.5‰ (June 2018) and 21.4‰ (March 2019, Figure 3C). The respective $\delta^{18}O$ value for surface water sulfate ranged between 11.5‰ and 13.0‰. The $\delta^{34}S$ value of surface water sulfate at Brejo do Espinho was scattered around 22.6 ± 0.3‰ (2 S.D.; *n* = 9; Figure 3B; Supplementary Table S1), independent of seasonality. The $\delta^{18}O$ value for surface water sulfate at Brejo do Espinho varied between 15.9‰ and 18.0‰.

Figure 3. Annual cycles of surface water in Lagoa Vermelha (black signatures) and Brejo do Espinho (red signatures) samples from different locations collected in March 2018 are comprised in the black and red brackets. (**A**) Sulfate concentrations. Data from [29] are in broad agreement with the present data; (**B**) $\delta^{18}O$ values of dissolved sulfate from surface water; (**C**) $\delta^{34}S$ values of dissolved sulfate. Error bars represent the external reproducibility (2 S.D.).

Figure 4. Pore-water data from different cores taken from Lagoa Vermelha and Brejo do Espinho. The light blue dashed lines represent the respective seawater values. (**A**) Sulfate concentrations in Lagoa Vermelha; (**B**) sulfate concentrations in Brejo do Espinho; (**C**) $\delta^{34}S$ of dissolved sulfate in Lagoa Vermelha; (**D**) $\delta^{34}S$ of dissolved sulfate in Brejo do Espinho; (**E**) $\delta^{18}O$ of dissolved sulfate in Lagoa Vermelha; (**F**) $\delta^{18}O$ of dissolved sulfate in Brejo do Espinho.

In March 2018, surface water at Lagoa Vermelha showed a mean sulfate concentration of 47 mM with a δ^{34}S value of 20.7‰ and a mean δ^{18}O value of 12.6‰ (Figure 3, Supplementary Table S1). For Brejo do Espinho, a mean sulfate concentration of 71 mM with an average δ^{34}S value of 22.6‰ and a δ^{18}O value of 15.5‰ (Figure 3, Supplementary Table S1) characterized the surface water at Brejo do Espinho in March 2018.

In Lagoa Vermelha, pore-water sulfate concentrations displayed an overall decrease from maximum values between 50 and 60 mM at 0.05 m to 30–50 mM downcore (Figure 4). For most cores, the respective δ^{34}S values showed a slight increase from 21‰ to approximately 25‰ with a maximum of 35.7‰ in the middle layer of core LV-E. The respective δ^{18}O$_{SO4}$ values slightly increased from 12‰ to 15‰ with maximum values of 18.7‰ in core LV-E. The cores LV-E and LV-D deviated from the average values seen in the other cores. LV-E is characterized by isotopically enriched values, while the most seaward core LV-D showed much less enriched values in all sulfur phases. In addition, LV-D did not show general trends throughout the core, as seen in the other cores (Figure 4). Within the upper 0.4 m sediment column, the sulfur isotopic composition of pore-water sulfide ranged between −27.0‰ and −12.0‰ (Supplementary Table S2).
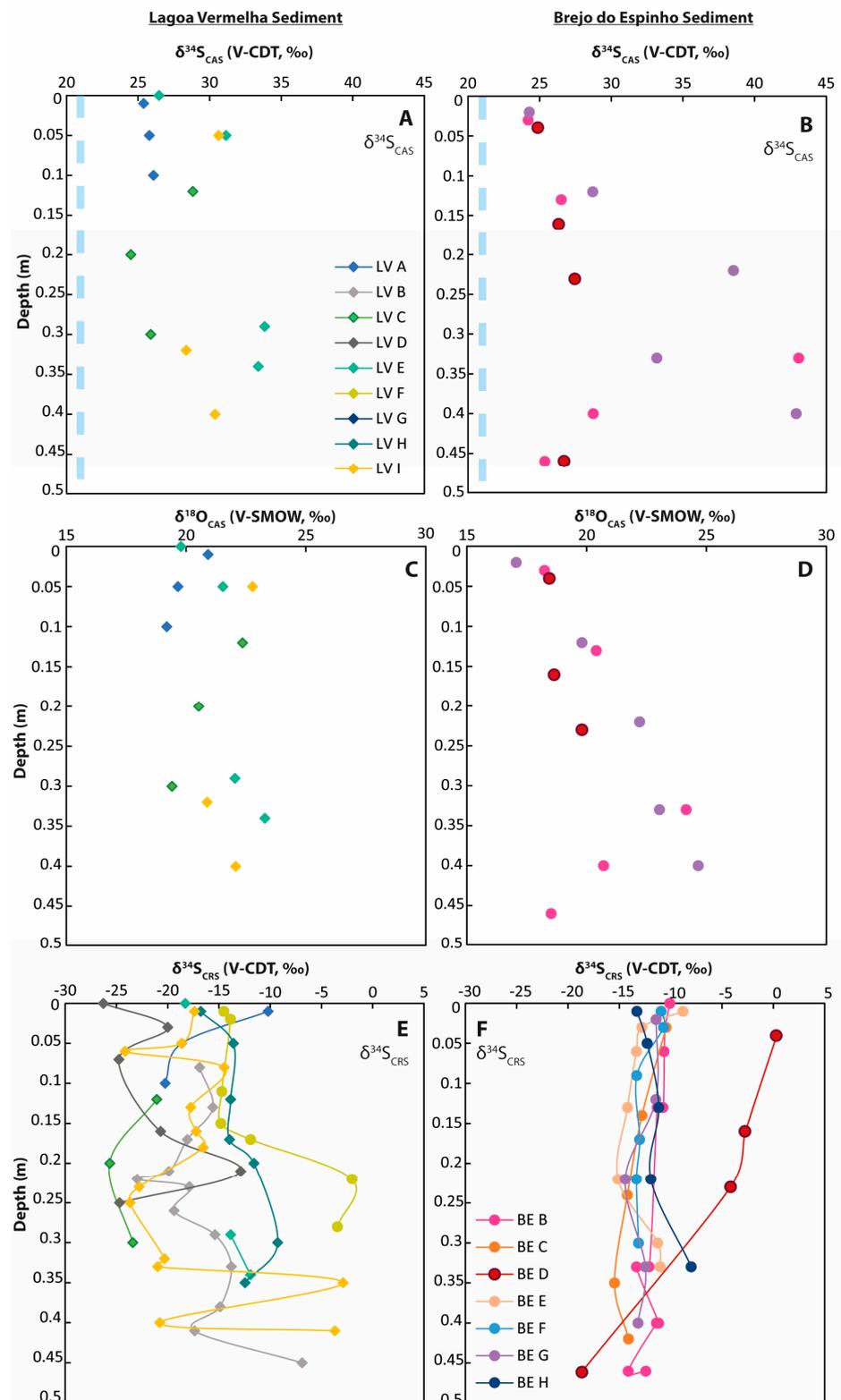
At Brejo do Espinho, there was a general trend towards higher pore-water sulfate concentrations from 70 to 160 mM with increasing sediment depth (Figure 4). The sulfur isotopic composition, as well as the oxygen isotopic composition for pore-water sulfate, were relatively invariant outside analytical standard deviation (2 S.D.), with a range from 22.5‰ to 25.7‰ for δ^{34}S and 15.2‰ to 19.1‰ for δ^{18}O (Figure 4, Supplementary Table S3). Only the pore-water sulfate at the seaward portion (BE-D) showed lower average δ^{34}S and δ^{18}O values, of 20.1‰ and 13.3‰, respectively. Hydrogen sulfide gas bubbles directly below the microbial mat had a mean δ^{34}S value of −21.9‰ (Supplementary Table S3). The sulfur isotopic composition of pore-water sulfide varied from −19.9‰ to −18.4‰ between the lagoon floor and 0.4 m sediment depth (Supplementary Table S3).

4.3. Geochemistry of Sediment Samples
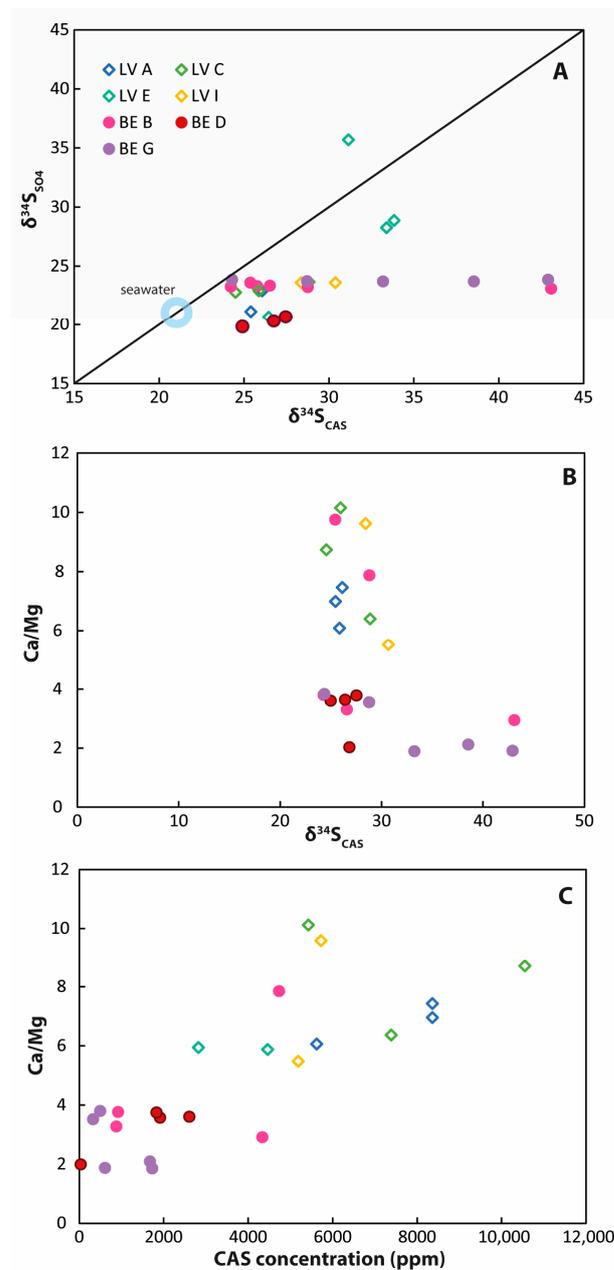
At Lagoa Vermelha, the firmground revealed a δ^{34}S$_{CAS}$ value of 27.8‰. Samples taken from a stromatolitic build-up yielded a similar δ^{34}S$_{CAS}$ value of 27.5‰. Downcore in the sediment, δ^{34}S$_{CAS}$ values increased from around 25‰ to more than 30‰ (Figure 5A). Carbonate sediment samples were characterized by δ^{18}O$_{CAS}$ values of 19.2‰ at the surficial sediment layer with values slightly increasing to a maximum of 23.3‰ at a 0.29 m sampling depth (Supplementary Table S2). Generally, the sulfur isotopic composition of sedimentary pyrite at Lagoa Vermelha showed a broad variation between −26.3‰ and −2.0‰ with a slight trend towards higher values downwards (Figure 5, Supplementary Table S2).

At Brejo do Espinho, the δ^{34}S$_{CAS}$ and δ^{18}O$_{CAS}$ values for carbonate sediment samples reached up to 43.1‰ and 24.7‰, respectively, but without showing a clear enrichment downcore (Figure 5, Supplementary Table S3). Most δ^{34}S$_{CRS}$ values varied between −15.5‰ and −8.0‰, while δ^{34}S$_{CRS}$ values from the seaward portion (BE-D) were more enriched in ^{34}S, with values between −4.2‰ and 0.3‰ within the first 0.23 m core depth (Figure 5, Supplementary Table S3). A weak trend towards lower values downcore might exist.

For Lagoa Vermelha samples, a nearly constant Mg/Ca molar ratio of about 0.2 was determined throughout the sediment core (Supplementary Table S2). Conversely, a higher Mg/Ca molar ratio of 0.5 at Brejo do Espinho characterized the upper sediment layer and increased to 0.9 at 0.4 m sampling depth (Supplementary Table S3). CAS concentrations of around 6000 ppm in the Lagoa Vermelha samples were more than threefold higher than in Brejo do Espinho samples, with a mean CAS value of 1700 ppm (Figure 6).

Figure 5. Sulfur and oxygen isotope values from CAS and pyrite (CRS fraction) from sediment cores. The light blue dashed lines represent the respective seawater values. Note that the marine value for $\delta^{18}O_{SO4}$ is lower (app. 10‰) than the displayed scale. (**A**) $\delta^{34}S_{CAS}$ values in Lagoa Vermelha sediment; (**B**) $\delta^{34}S_{CAS}$ values in Brejo do Espinho sediment; (**C**) $\delta^{18}O_{CAS}$ values in Lagoa Vermelha sediment; (**D**) $\delta^{18}O_{CAS}$ values in Brejo do Espinho sediment; (**E**) $\delta^{34}S_{CRS}$ values in Lagoa Vermelha sediment; (**F**) $\delta^{34}S_{CRS}$ values in Brejo do Espinho sediment.

Figure 6. Comparison of CAS data. (**A**) $\delta^{34}S_{CAS}$ values versus $\delta^{34}S$ values of pore-water from the same core depth. Most $\delta^{34}S_{CAS}$ values are significantly enriched compared with the $\delta^{34}S_{SO4}$ values; (**B**) a slight negative correlation—especially for samples from Brejo do Espinho—is visible for $\delta^{34}S_{CAS}$ values compared with the respective Ca/Mg ratios; (**C**) a positive correlation exists between the CAS concentration and the respective Ca/Mg ratio. Samples from Brejo do Espinho are characterized by lower CAS concentrations and high Ca/Mg ratios compared with samples from Lagoa Vermelha.

5. Discussion

5.1. Sulfur Cycling in Surface Water

5.1.1. Sulfate Concentrations—Controlled by Evaporation and Rain Events

On an annual scale, sulfate concentrations collected at the same sites in both lagoons ranged between 40 and 60 mM (Figure 3). These concentrations are consistent with the data reported in [29]. Even though these authors did not report the very high concentrations of more than 100 mM, determined in this study for January and March 2019 at Brejo do Espinho, they also reported maximum sulfate concentrations in March. All values generated for the present study exceeded the marine sulfate concentration of 28 mM and

indicate an enrichment due to evaporitic conditions. As for the data collected in March 2018, the generally higher sulfate concentrations in Brejo do Espinho can be explained by the permanently higher evaporation compared with the smaller water body than in Lagoa Vermelha.

Sulfate concentrations in surface water samples collected in March 2018 were highly variable for Brejo do Espinho (between 33 and 80 mM) and more homogenous in Lagoa Vermelha (between 44 and 50 mM). The lowest value in Brejo do Espinho (33 mM) was measured at the seaward side above the core BE-D; it is likely influenced by seawater influence from below. No trend to higher sulfate concentrations landwards was discernible for the other samples in Brejo do Espinho (54 to 80 mM). Possible explanations for the remarkable heterogeneity in sulfate concentrations are: (1) during ocean swells generated by off-shore storms, large amounts of seawater are pumped into the lagoons; and (2) daily evaporation rates over three rain-free weeks could influence the sulfate concentrations in the max. 30 cm deep surface water of Brejo do Espinho. Wet, muddy areas around the Brejo do Espinho proved the progressing evaporation of lagoonal water that had started prior to fieldwork for this study. Lagoa Vermelha is up to 2 m deep and is not surrounded by salt pans; thus, did not show such intense loss in size.

Although sulfate concentrations measured for March 2018 were consistent with those published in [29], they are not exclusively typical for that time of the year. Instead, sulfate concentrations can reach much higher values, as shown by the data from the following year (November 2018–March 2019). Variations were stronger in the smaller Brejo do Espinho, with sulfate concentrations of more than 100 mM, and weaker in the larger Lagoa Vermelha, with sulfate concentrations of more than 50 mM (Figure 3). Notably, even though the period between November to March is the wet season [34], it is also the hottest time of the year, with a dynamic change between freshwater influence and evaporation. In [35], it was observed that single rain events can significantly influence the annual evaporation–precipitation balance of those lagoons. Together with the fact that within the same month, sulfate concentrations can significantly vary (see March 2018 in Figure 3; Supplementary Table S1), it becomes clear that the exact sampling time is vital even with no rain. This is especially true for the smaller Brejo do Espinho, which responds more strongly to evaporation and rain events.

5.1.2. Sulfur and Oxygen Isotopes—Influenced by BSR, Sulfur Oxidation, and Evaporation

Sulfur isotope values of dissolved sulfate between 20.5‰ and 22.7‰ in both lagoons were similar or up to 1.7‰ higher than the contemporary seawater value of +21.0‰ [40,41], which is consistent with former studies [16,29], and confirms the general dominant impact of seawater on the composition of lagoonal water [12]. The respective oxygen isotope values were, however, enriched by up to 2‰ in Lagoa Vermelha, and up to more than 5‰ in Brejo do Espinho compared with seawater [41,42].

The ^{34}S, and partially, the ^{18}O isotope enrichment of dissolved sulfate, results from the metabolism of sulfate-reducing bacteria in the anoxic sediment with a limited exchange between lagoonal water and water supply from the sea or Lagoa Araruama. BSR is a strictly anaerobic process [43,44] and does not occur in oxygen-saturated surface water. The preferred reduction of the isotopically lighter ^{32}S^{16}O$_4^{2-}$ ultimately leads to an enrichment of ^{34}S and ^{18}O in the remaining sulfate [45–49]. Consequently, there must be an upward water flux from anoxic pore-water to the lagoonal surface water; otherwise, the sulfate in the oxygenated surface water of Brejo do Espinho did not exhibit the observed isotopic enrichment. Gas bubbles that had diffused upwards and accumulated below the microbial mats in Brejo do Espinho contained H$_2$S with an isotope value of −21.9‰ (Supplementary Table S1). This confirms the ubiquitous impact of BSR in the pore-water on oxidized and reduced sulfur in the surface water. The majority of the upwardly diffused and isotopically depleted H$_2$S is, however, expected to be re-oxidized by anaerobic or aerobic microbes to either intermediate sulfur species or sulfate within the uppermost centimeter of the sediment [50–53]. The repeated oxidation of sulfide and intermediate sulfite releases

isotopically depleted sulfate back into the surface water and buffers any further sulfur isotope enrichment of sulfate. Additionally, the oxidation processes influence the $\delta^{18}O_{SO4}$ values [42,54–56]. Indeed, the respective $\delta^{18}O_{SO4}$ values of the dissolved sulfate in Brejo do Espinho surface water were enriched in ^{18}O by more than 5‰ (March 2018: 15.5‰; annual: 15.9–18‰) compared with seawater sulfate values (9.3 to 10.5‰; [42,57]). In [16], similar isotope values for the surface water in Brejo do Espinho were reported, and an equilibrium state of $\delta^{18}O_{SO4}$ was proposed, approaching the $\delta^{18}O$ value of atmospheric oxygen (24.1‰; [58,59]) due to repeated sulfur oxidation. In contrast to the $\delta^{18}O_{SO4}$ in Brejo do Espinho, the $\delta^{18}O_{SO4}$ in Lagoa Vermelha was enriched by no more than 2‰ (Figure 3). The values indicate a lower degree of upward diffusion and the re-oxidation of sulfur. The fact that the respective $\delta^{34}S_{SO4}$ values for the Lagoa Vermelha surface water were close to the seawater value of 21‰ did not necessarily reflect a lower degree of BSR occurring in the pore-water, as suggested by [29], but may be due to the lower upward diffusion rate of pore-water.

Apart from BSR in the pore-water and sulfur oxidation near the water surface, the isotopic exchange between oxygen isotopes of sulfate and water during sulfur metabolizing processes should be considered as the third controlling factor for $\delta^{18}O_{SO4}$ values in the surface water [46,54,60–62]. For lagoonal water with temperatures around 30 °C, a $\delta^{18}O_{H2O}$ value of 6–7‰ can be assumed [63–65]. This isotopic value increases with increasing temperatures and the rate of evaporation. Considering the higher temperatures in the Brejo do Espinho, the higher $\delta^{18}O_{SO4}$ values in the surface water follow the higher $\delta^{18}O_{H2O}$ values.

5.2. Pore-Water: Two Types of Sulfur Cycling

Sulfate sulfur isotope data higher than 21‰ indicated ongoing BSR in the pore-water in both lagoons (Figure 4). Although progressive BSR contributes to ^{34}S enrichment in residual pore-water sulfate in the deeper sediment layers, BSR is not the only controlling factor for sulfate concentrations in the upper 0.4 m of the lagoonal sediments. Both lagoons exhibit pore-water sulfate concentrations that are mostly higher than seawater values due to the intense evaporation of the surface water. When comparing the sulfate concentrations of both lagoons, two types of $\delta^{34}S_{SO4}$ and the $\delta^{18}O_{SO4}$ pore-water profiles can be distinguished.

The first type of pore-water profile is characteristic of most sites sampled in Lagoa Vermelha: sulfate concentrations slightly decreased from maximum values between 50 and 60 mM at 0.05 m to 30–50 mM at 0.45 m. All sulfate concentrations were higher than average seawater sulfate concentrations, which could be explained by the diffusion of dense saline water into the pore-water. The combination of slightly decreasing sulfate concentrations with slightly increasing $\delta^{34}S_{SO4}$ (from 21‰ to approximately 25‰) and $\delta^{18}O_{SO4}$ (from 12‰ to 15‰ and higher) values with depth indicates ongoing BSR. In principle, maximum sulfate concentrations at 0.05 m depth could also reflect intensified sulfur oxidation in the suboxic zone; however, the respective $\delta^{34}S_{SO4}$ values were not depleted in ^{34}S. In summary, the values at 0.05 m likely reflect the accumulation of highly saline water.

The second pore-water profile type was typical for most pore-water profiles measured at Brejo do Espinho. Those profiles (Figure 4; cores BE C, G, F) show highly varying sulfate concentrations with a continuous trend from values between 50 and 80 mM at the top towards even higher values of 70 to more than 100 mM at depth. The $\delta^{34}S_{SO4}$ values in these pore-waters broadly ranged between 23‰ and 25‰; however, no significant increase with depth was discernible.

The increase from high (compared with a seawater value of 28 mM) to very high sulfate concentrations downcore cannot solely be explained by downward diffusion. Rather, intense surface water evaporation is proposed to stimulate a thermohaline circulation of the pore-water. This way, highly saline, dense surface water flows downward into the sediment and causes an increase in the pore-water sulfate concentration within the lagoonal sediment, similar to the formation of a brine lens. Subsurface inflow from neighboring Lagoa Araruama in the north, or seawater in the south, could have caused further fluctuations in sulfate concentrations in the vertical profiles. As a result of the downward flow of a heavy

brine, less saline pore-water migrates upward. Sulfate in this water was enriched in ^{34}S as a result of BSR. Consequently, the surface water showed enriched $\delta^{34}S_{SO4}$ values (see Section 5.1). The fact that the $\delta^{34}S_{SO4}$ values in the pore-water profiles (Figure 4D) showed hardly any increase with depth, but instead appeared quite homogenous (except BE D and H) can now be explained as follows: a progressive increase in $\delta^{34}S_{SO4}$ with depth as the consequence of ongoing BSR in the pore-water would only be expected when pore-water sulfate is continuously consumed, and the only sulfate source is diffusion from above. However, the proposed downward flux of saline, sulfate-rich water initiated fluid exchange at Brejo do Espinho, homogenizing its sulfur isotope values.

The respective $\delta^{18}O_{SO4}$ values were strongly enriched in ^{18}O compared with seawater sulfate and increase slightly with depth from 16–18‰ at the core top to 17–19‰ at the core bottom (Figure 4F). The enriched $\delta^{18}O_{SO4}$ values in the pore-water sulfate reveal several processes: first, the slight increase in δ^{18}O values downcore could reflect progressing BSR because sulfate-reducing bacteria favor $^{32}S^{16}O^{2-}$ over $^{32}S^{18}O^{2-}$ [45,60,66]; second, and similar to the $\delta^{18}O_{SO4}$ values in the surface water, the general enrichment in ^{18}O compared with modern seawater sulfate and the $\delta^{18}O_{SO4}$ values at Lagoa Vermelha might reflect the exchange of oxygen between sulfate and the evaporative water enriched in ^{18}O [67,68]. The thermohaline circulation must enhance bacterial sulfur oxidation by bringing hypersaline surface water further downwards and sulfide-rich anoxic water upwards to the suboxic zone, where most sulfide-oxidizing microbes live. Numerous studies suggest that the microbial recycling of ambient sulfate via back-reactions facilitates the exchange of oxygen from sulfoxyanion intermediates and/or sulfite with ambient water [54–56,69,70]. Further evidence for ongoing sulfur oxidation in Brejo do Espinho pore-water is provided by a lower pH of 7.1 compared with 8.8 in the surface water [29], and by a 15% higher SO_4^{2-}/Cl^- ratio in Brejo do Espinho compared with seawater [16]. Thus, from the present results, it can be proposed that the isotopic exchange with ^{18}O-enriched pore-water during sulfur metabolizing processes contributes to the observed ^{18}O-enrichment in sulfates of the Brejo do Espinho pore-water.

This is similar to [16], in which an upward advective process driven by evaporation, as described above, was proposed. However, these authors proposed a contribution of Mg-rich subsurface fluids from the adjacent Lagoa Araruama into the pore-waters of Brejo do Espinho. The downward fluid flow into the Brejo do Espinho pore-waters is proposed here as an alternative.

In the absence of burrowing organisms, and hence, bioturbation, in Brejo do Espinho, the proposed thermohaline circulation between surface and pore-water represents a mechanism for transporting sulfate down into the sediment and, as a consequence, significantly enlarges the zone of ongoing BSR. This is remarkable since, for marine sediments, it is assumed that without bioturbation and diffusion only, the dissolved sulfate would have been consumed by sulfate reducers within the top 0.2 m [53]. An example is the Løgten Lagoon (Denmark), which exhibits sulfate exhaustion in the upper 10 cm (top: 13 mM; [71]). In contrast, the hypersaline Solar Lake (Egypt) and the sabkha in Abu Dhabi exhibited a similar pore-water pattern to Brejo do Espinho, with slightly increasing sulfate concentrations and more or less invariant $\delta^{34}S_{SO4}$ values in the upper 8 cm (Solar Lake) and 30 cm (Abu Dhabi sabkha) [65,71].

In summary, in the larger Lagoa Vermelha, the usual pattern of BSR in marine sediments was discernible, while the pore-water profiles of the smaller Brejo do Espinho were influenced by intense evaporation and thermohaline circulation. In the smaller lagoon, the degree of BSR cannot simply be inferred from the $\delta^{34}S_{SO4}$ in pore-water, as the diffusion of pore-water with a sulfur oxidation signature can mask the pure BSR signature. Extreme evaporation drives the thermohaline circulation of lagoonal water. This enables downward sulfate migration into the sediment and homogenization of the δ^{34}S signature of sulfate between pore-water and the isotopically enriched surface water. Notably, the data are only representative of March. If thermohaline circulation greatly affects the pore-water chemistry, pore-water profiles at Brejo do Espinho could exhibit a significant seasonality.

Consequently, the two types of pore-water profiles described above represent "endmember" settings of two different lagoonal environments, variable in time and space, and complex in terms of the processes involved.

5.3. δ^{34}S in Pyrite Revealing Differences in Sulfur Cycling

For both lagoonal settings, the δ^{34}S values of pyrite reflected the corresponding pore-water types, as observed from the dissolved sulfate data. In the case of Lagoa Vermelha, most cores showed variable δ^{34}S$_{CRS}$ values between -2‰ and -27‰, with a weak tendency towards enriched values downwards (Figure 5E). The slightly increasing δ^{34}S$_{CRS}$ values reflected the proceeding BSR in an increasingly ^{34}S-enriched sulfate pool, consistent with the sulfur and oxygen isotope values in the dissolved sulfate. The majority of the Brejo do Espinho cores showed more homogenous δ^{34}S$_{CRS}$ values between -10‰ and -15‰ (Figure 5F). These values were mostly consistent with the pore-water data, which reflected pore-water homogenization due to thermohaline circulation. The weak trend toward lower δ^{34}S$_{CRS}$ values downwards can result from a more open sulfate pool or a decreased rate of BSR, reflecting the successive consumption of easily degradable organic matter. Elevated rates of BSR have been described from hypersaline lagoons and are driven by warm temperatures, high sulfate concentrations, and organic-rich sediments [71–75]. A high BSR rate is associated with lower sulfur isotope fractionation, based on less channeled sulfide through the microbial pathway and higher sulfide oxidation [76]. Additionally, a more open sulfate pool from the marine side is possible, too, following observations by former studies [12,16]. A subsurface connection to the Lagoa Araruama, north of Brejo do Espinho, can be excluded. This is because Brejo do Espinho dries out during the dry season, starting from the northern to the southern seaward shelf.

Similarly to dissolved pore-water sulfate and CAS, the dissolved sulfide phase showed lower sulfur isotope values than mineral pyrite. At Lagoa Vermelha, the δ^{34}S values of dissolved sulfide from bulk cores ranged between -27‰ and -12‰. In Brejo do Espinho, dissolved sulfide δ^{34}S values ranged between -21.9‰ and -18.4‰. One possible explanation could be a general long-term decrease in the sulfur isotopic composition of the total sulfur pool in both lagoons. A stronger influence of meteoric fluids or seawater lasting for several annual cycles can add isotopically lighter sulfur to the lagoonal systems. At this moment, the minerals would reflect a slightly older sulfur isotope signal, while the pore-water would reflect the current state with isotopically lighter sulfur in the system. An alternative model [77] suggests that carbonate and pyrite precipitate in semi-enclosed microenvironments that are only partially representative of the bulk pore-water. BSR taking place in a (semi-)closed system not only leads to enriched δ^{34}S$_{SO4}$ values, as described above for the CAS, but also causes successive isotope enrichment of the reduced sulfide. Precipitated pyrite arguably preserves this enriched sulfur isotope signal.

Most δ^{34}S values of all analyzed sulfur phases were generally more enriched in ^{34}S in Brejo do Espinho compared with Lagoa Vermelha, which can be explained by progressing Rayleigh fractionation caused by BSR in a smaller sulfate pool. Indeed, Brejo do Espinho is smaller (1 km^2) than Lagoa Vermelha (2 km^2). The isotopic enrichment of all sulfur phases in Brejo do Espinho indicates at least a partially restricted sulfate pool. This sulfur isotope enrichment implies the existence of a strong sink where isotopically light sulfur can leave the lagoonal sulfur pool. Sulfide resulting from BSR either leaves the sediment as volatile H$_2$S (g) or re-oxidizes in marine sediments; the primary sink for isotopically light sulfur is sedimentary pyrite. In the Brejo do Espinho, however, this pyrite shows a weaker ^{34}S depletion than the pyrite in Lagoa Vermelha. Another optional and possibly underestimated sink for isotopically light sulfur might be the diffusional loss of H$_2$S. Below the microbial mats of Brejo do Espinho, H$_2$S bubbles accumulate. Brejo do Espinho is extremely shallow (in March it was 20 cm deep); therefore, the diffusional loss of H$_2$S into the atmosphere can contribute to isotope enrichment of the sulfur pool of the very shallow Brejo do Espinho lagoon.

5.4. Carbonate-Associated Sulfate (CAS) Showing Different Formation Environments for Ca/Mg and Ca Carbonates

The CAS values in both lagoons do not simply reflect the different pore-water patterns (Figure 5). Instead, the CAS sulfur isotope values scatter between 24.2‰ and 43.1‰ at Brejo do Espinho and from 24.5‰ to 33.8‰ at Lagoa Vermelha. When comparing the isotope data from all cores sampled together, a downwards tendency towards higher sulfur and oxygen isotope values is visible (Figure 5). For Lagoa Vermelha, this increase followed the development of ^{34}S-enriched pore-water with increasing depth. It is therefore consistent with other data suggesting ongoing BSR and isotopically evolving pore-water. For Brejo do Espinho, increasing $\delta^{34}S_{CAS}$ values could be confirmed for one (BE-G) of the three analyzed cores. BE-B exhibited high variability, but towards the bottom of the core, the δ^{34}S values decreased again. The most seaward core, BE-D, showed no change at all. In this context, notably, two of the seven cores analyzed for CAS exhibited values for all parameters that did not represent steadily proceeding BSR with depth (BE-D, the most seaward core, and LV-E, which showed extreme isotopic enrichment for all sulfur phases). The high $\delta^{18}O_{CAS}$ values reflect the different processes that influence dissolved sulfate in the pore-water, including progressing BSR, repeated sulfide and intermediate sulfur oxidation, and oxygen isotope exchange between intermediate sulfur phases and ^{18}O-enriched water. Moreover, the enriched $\delta^{18}O_{CAS}$ values at the core tops also indicate multiple redox stages of the sulfate before incorporation into the carbonate.

At first sight, the highly enriched sulfur isotope values (>30‰) for some CAS samples appear surprising, given the extremely high sulfate concentrations and the $\delta^{34}S_{SO4}$ values $\leq$ 25‰ in the pore-water. In order to understand those $\delta^{34}S_{CAS}$ values, it is crucial to consider different formation mechanisms of carbonate minerals with different magnesium concentrations. For calcite that is not dependent on the presence of EPS, it was shown that CAS reflected the bulk- or seawater sulfur isotope signature [33]. For dolomite, however, it was shown here and in prior studies that the $\delta^{34}S_{CAS}$ value reflects microbial metabolic processes and cannot be used as a proxy for the normal marine signature [78,79]. The analyzed samples were bulk samples reflecting different mixtures of calcian and Mg-rich carbonates (Figure 6B,C; Supplementary Tables S2 and S3). The extremely high $\delta^{34}S_{CAS}$ and $\delta^{18}O_{CAS}$ values can be correlated to Ca/Mg ratios < 3 in the carbonate, i.e., towards Mg-enriched carbonates (Figure 6), arguably representing non-stochiometric dolomite [22].

Ca/Mg carbonate precipitation in Lagoa Vermelha and Brejo do Espinho was proposed to result from the direct mediation of SRB [72]. Even if these Ca/Mg carbonates are poorly ordered and non-stoichiometric, they still might act as precursors for later, better-ordered dolomite in the sense of Ostwald's step rule [11,73]. More recent studies have proven carbonate nucleation within the EPSs of sulfur-metabolizing bacteria, and concluded that EPSs play a key role in Mg incorporation into carbonate [65,72,74]. An increased saturation state characterizes EPSs for Ca/Mg carbonate, high alkalinity, increased pH, and available, dehydrated Mg [19,24,80–82]. In [11], it was suggested that the high degree of evaporation may promote ecological stress on microbes, which causes the production of EPS to protect them from desiccation, salinity, and solar radiation. Therefore, the higher salinity at Brejo do Espinho might be a prerequisite to produce sufficient EPSs, which serve as the microenvironment where Ca/Mg carbonate can nucleate. In this microenvironment with different chemical conditions from the surrounding bulk pore-water, BSR can reduce the sulfate concentrations, thereby driving Rayleigh fractionation and increasing $\delta^{34}S_{CAS}$ and $\delta^{18}O_{CAS}$ values. Consequently, $\delta^{34}S_{CAS}$ values from Ca/Mg carbonate samples do not represent the ambient bulk pore-water but—depending on the relative Ca/Mg carbonate proportion of the bulk sample—more and more represent the adjacent fluid in this particular microenvironment. The samples discussed here were bulk rock samples; therefore, we propose that a CAS analysis in the separated Mg-rich carbonate phase would likely reveal even higher $\delta^{34}S_{CAS}$ values than those presented in this study.

In contrast to Mg-rich carbonate, lagoonal calcite and aragonite neither require the presence of EPS and very high seawater alkalinity nor the presence of microbes. There-

fore, the samples with Ca/Mg ratios > 3 had rather higher CAS concentrations and lower $\delta^{34}S_{CAS}$ values, closer to the $\delta^{34}S_{SO4}$ values in the pore-water (Figure 6). However, even some of the Mg-poorer samples showed enriched $\delta^{34}S_{CAS}$ values in both lagoons. Those enriched $\delta^{34}S_{CAS}$ values might reflect seasonal variations in the activity of distinct sulfur-metabolizing microbes. Water chemistry and evaporation change from dry to wet seasons, and probably influence microbial activity and, therefore, the isotopic composition of dissolved sulfate. It thus seems possible that the $\delta^{34}S_{SO4}$ values in the pore-waters of both lagoons were higher than 25‰ during other months from March, and then matched the $\delta^{34}S_{CAS}$ values that were higher than 25‰. Indeed, for Lagoa Vermelha, previous studies have proposed dolomite precipitation to mainly occur in May and June, a time of high salinity and the required saturation state for dolomite precipitation in the pore-water [22,29]. Dolomite formation temperatures of 32 to 34 °C ($\pm$1.6 °C) were determined by clumped isotope data [21]. For Brejo do Espinho, however, [29] proposed continuous precipitation throughout the year. Therefore, seasonal changes in pore-water isotopic composition are probably not the (primary) controlling factors for the high $\delta^{34}S_{CAS}$ values.

5.5. More Implications on Lagoonal Ca/Mg Carbonate Formation

The $\delta^{34}S$ and $\delta^{18}O$ values for pore-water sulfate and CAS provide several lines of evidence leading to Ca/Mg carbonate formation. First, $\delta^{18}O$ values in the pore-water suggest higher rates of sulfide and intermediate sulfur oxidation within the sediment column of Brejo do Espinho. Sulfur oxidation leads to lower pH, a preferential dissolution of calcite, and ultimately, to the relative enrichment of Ca/Mg carbonates in the sediment column [83]. Ref. [16] proposed that intense sulfide oxidation in both lagoons enabled undersaturation for Mg-calcite and aragonite and supersaturation for dolomite. In the present study, a stronger influence of sulfur oxidation on the $\delta^{18}O$ values was observed in Brejo do Espinho compared with Lagoa Vermelha. This is consistent with generally lower Ca/Mg ratios in the Brejo do Espinho samples compared with the Lagoa Vermelha samples. Therefore, sulfur oxidation appears to be a requirement for achieving the relative enrichment of Ca/Mg carbonate in the sediment. A further consequence is the stimulation of enhanced rates of carbonate recrystallization and dissolution, which is a key part of early diagenesis. The incorporation of Mg occurs during carbonate diagenesis; thus, the higher recrystallization rate is another factor promoting the successive relative enrichment of Ca/Mg carbonate in the sediment.

Second, with increasing Mg contents, the $\delta^{34}S_{CAS}$ values no longer represented the ambient bulk water, but represented the EPS microenvironment more and more. This finding may have implications for using dolomite CAS data for reconstructing the isotopic composition of seawater sulfate in the geological past. Within the clear limitations of correlations between Earth's recent and deep time, Lagoa Vermelha has been considered an "analogue" for sedimentary Ca/Mg carbonate formation during periods of the Precambrian [17]. Similar to the $\delta^{34}S_{CAS}$ data of the present study, Precambrian sulfur isotope data are, in part, very high and remarkably variable [84,85]. The results of the present study suggest that the option should be considered that the highly variable $\delta^{34}S_{CAS}$ values in these rocks are not representative of a marine signal (or diagenesis), but rather reflect the microenvironment in which these dolomites formed. More work is required to support or reject this hypothesis.

6. Conclusions

The analysis of sulfur and oxygen isotope ratios in water and sediment samples from Lagoa Vermelha and Brejo do Espinho lagoons revealed differences in sulfur cycling and provides relevant insight into processes driving sedimentary Ca/Mg carbonate formation. Due to its smaller size (1 km^2 with an average depth of <0.5 m), the Brejo do Espinho faces more intense evaporation, which triggers water circulation with heavy evaporative saline surface water migrating downwards and, as a consequence, pore-water moving upwards. A saline water flow influences the microbial processes, affecting sulfur redox cycles in

the pore space. Very high $\delta^{34}S_{CAS}$ values in samples with the highest Mg concentrations (Ca/Mg < 3) indicated microenvironments favoring the precipitation of very-high-Mg calcite and calcian dolomites. Abundant EPS, a result of high microbial activity and response to high salinity in the pore-water, may represent this microenvironment and act as a site of Ca/Mg carbonate nucleation. The corresponding increase in $\delta^{34}S_{CAS}$ in the Mg-rich samples confirms the nucleation in such a microenvironment. At least for both lagoons from this study, Ca/Mg carbonate appears to be an archive for early diagenetic microbial activity in pore-water rather than for the surface water above the sediment. The present data emphasize the different formation conditions under which calcite and dolomite form within the sediment column.

Although it is impossible to determine the relative significance of sulfate reduction, sulfide oxidation, and sulfur disproportionation, the increased $\delta^{18}O_{SO4}$ values in both the surface and pore-water of Brejo do Espinho indicate increased rates of sulfur oxidation. The alternation between BSR and sulfur oxidation probably leads to a higher precipitation–dissolution rate and a faster development of early diagenetic characteristics in the carbonate, such as Mg incorporation. Future work must explore to what extent a higher precipitation–dissolution rate and alternation between sulfur oxidation and sulfate reduction influence the rate in which Ca–Mg carbonate minerals reach a stable state, making them more resistant against dissolution. High salinity, vertical water circulation, and a lack of bio-irrigation, particularly in the Brejo do Espinho lagoon, might offer alternative interpretations for the highly variable $\delta^{34}S_{CAS}$ values typical of many Precambrian carbonates.

References

1. Given, R.K.; Wilkinson, B.H. Dolomite abundance and stratigraphic age; constraints on rates and mechanisms of Phanerozoic dolostone formation. *J. Sed. Res.* **1987**, *57*, 1068–1078. [CrossRef]
2. Warren, J. Dolomite: Occurrence, evolution and economically important associations. *Earth-Sci. Rev.* **2000**, *52*, 1–81. [CrossRef]
3. Tucker, M.E. Precambrian dolomites: Petrographic and isotopic evidence that they differ from Phanerozoic dolomites. *Geology* **1982**, *10*, 7–12. [CrossRef]
4. Grotzinger, J.P. Facies and evolution of Precambrian carbonate depositional systems: Emergence of the modern platform archetype. In *Controls on Carbonate Platforms and Basin Development*; SEPM Special Publications: Tulsa, OK, USA, 1989; Volume 44, pp. 79–107.

5. Chang, B.; Li, C.; Liu, D.; Foster, I.; Tripati, A.; Lloyd, M.K.; Maradiaga, I.; Luo, G.; An, Z.; She, Z.; et al. Massive formation of early diagenetic dolomite in the Ediacaran ocean: Constraints on the "dolomite problem". *Proc. Natl. Acad. Sci. USA* **2020**, *117*, 14005–14014. [CrossRef]

6. Schmoker, J.W.; Krystink, K.B.; Halley, R.B. Selected characteristics of limestone and dolomite reservoirs in the United States. *Am. Assoc. Petrol. Geol. Bull.* **1985**, *69*, 733–741.

7. Lumsden, D.N. Secular variations in dolomite abundance in deep marine sediments. *Geology* **1985**, *13*, 766–769. [CrossRef]

8. Holland, H.D.; Zimmerman, H. The dolomite problem revisited. *Int. Geol. Rev.* **2000**, *42*, 37–41. [CrossRef]

9. Gaines, A.M. Protodolomite redefined. *J. Sediment. Petrol.* **1977**, *47*, 543–546.

10. Gregg, J.M.; Bish, D.L.; Kaczmarek, S.E.; Machel, H.G. Mineralogy, nucleation and growth of dolomite in the laboratory and sedimentary environment: A review. *Sedimentology* **2015**, *62*, 1749–1769. [CrossRef]

11. Petrash, D.A.; Bialik, O.M.; Bontognali, T.R.R.; Vasconcelos, C.; Roberts, J.A.; Mckenzie, J.A.; Konhauser, K.O. Microbially catalyzed dolomite formation: From near-surface to burial. *Earth-Sci. Rev.* **2017**, *171*, 558–582. [CrossRef]

12. Vasconcelos, C.; Mckenzie, J.A. Microbial mediation of modern dolomite precipitation and diagenesis under anoxic conditions (Lagoa Vermelha, Rio de Janeiro, Brazil). *J. Sed. Res.* **1997**, *67*, 378–390.

13. Wright, D.T. The role of sulphate-reducing bacteria and cyanobacteria in dolomite formation in distal ephemeral lakes of the Coorong region, South Australia. *Sediment. Geol.* **1999**, *126*, 147–157. [CrossRef]

14. Wright, D.T.; Wacey, D. Precipitation of dolomite using sulphate reducing bacteria from the Coorong Region, South Australia: Significance and implications. *Sedimentology* **2005**, *52*, 987–1008. [CrossRef]

15. Warthmann, R.; van Lith, Y.; Vasconcelos, C.; McKenzie, J.A.; Karpoff, A.M. Bacterially induced dolomite precipitation in anoxic culture experiments. *Geology* **2000**, *28*, 1091–1094. [CrossRef]

16. Moreira, N.F.; Walter, L.M.; Vasconcelos, C.; Mckenzie, J.A.; McCall, P.J. Role of sulfide oxidation in dolomitization: Sediment and pore-water geochemistry of a modern hypersaline lagoon system. *Geology* **2004**, *32*, 701–704. [CrossRef]

17. Vasconcelos, C.; Warthmann, R.; Mckenzie, J.A.; Visscher, P.T.; Bittermann, A.G.; van Lith, Y. Lithifying microbial mats in Lagoa Vermelha, Brazil: Modern Precambrian relics? *Sed. Geol.* **2006**, *185*, 175–183. [CrossRef]

18. Sánchez-Román, M.; Vasconcelos, C.; Schmid, T.; Dittrich, M.; McKenzie, J.A. Aerobic microbial dolomite at the nanometer scale: Implications for the geologic record. *Geology* **2008**, *36*, 879–882. [CrossRef]

19. Krause, S.; Liebetrau, V.; Gorb, S.; Sánchez-Román, M.; McKenzie, J.A.; Treude, T. Microbial nucleation of Ca/Mg dolomite in exopolymeric substances under anoxic modern seawater salinity: New insight into an old enigma. *Geology* **2012**, *40*, 587–590. [CrossRef]

20. Bontognali, T.R.R.; McKenzie, J.A.; Warthmann, R.J.; Vasconcelos, C. Microbially influenced formation of Mg-calcite and Ca-dolomite in the presence of exopolymeric substances produced by sulfate-reducing bacteria. *Terra Nova* **2014**, *26*, 72–77. [CrossRef]

21. Bahniuk, A.; Mckenzie, J.A.; Perri, E.; Bontognali, T.R.R.; Vögeli, N.; Rezende, C.E.; Rangel, T.P.; Vasconcelos, C. Characterization of environmental conditions during microbial Ca/Mg carbonate precipitation and early diagenetic dolomite crust formation: Brejo do Espinho, Rio de Janeiro, Brazil. *Geol. Soc. London Spec. Publ.* **2015**, *418*, 243–259. [CrossRef]

22. Areias, C.; Barbosa, C.F.; Cruz, A.P.S.; McKenzie, J.A.; Ariztegui, D.; Eglinton, T.; Haghipour, N.; Vasconcelos, C.; Sánchez-Román, M. Organic matter diagenesis and precipitation of Ca/Mg carbonate and dolomite in modern hypersaline lagoons linked to climate changes. *Geochim. Cosmochim. Acta* **2022**, *337*, 14–32. [CrossRef]

23. Han, Y.J.; Aizenberg, J. Effect of magnesium ions on oriented growth of calcite on carboxylic acid functionalized self-assembled monolayer. *J. Am. Chem. Soc.* **2003**, *125*, 4032–4033. [CrossRef] [PubMed]

24. Arp, G.; Reimer, A.; Reitner, J. Microbialite formation of increased alkalinity, Satonda Crater Lake, Indonesia. *J. Sediment. Res.* **2003**, *73*, 105–127. [CrossRef]

25. Kwak, S.-Y.; DiMasi, E.; Han, Y.-J.; Aizenberg, J.; Kuzmenko, I. Orientation and mg incorporation of calcite grown on functionalized self-assembled monolayers: A synchrotron X-ray study. *Cryst. Growth Des.* **2005**, *5*, 2139–2145. [CrossRef]

26. Zhang, F.; Xu, H.; Konishi, H.; Kemp, J.M.; Roden, E.E.; Shen, Z. Dissolved sulfide-catalyzed precipitation of disordered dolomite: Implications for the formation mechanism of sedimentary dolomite. *Geochim. Cosmochim. Acta* **2012**, *97*, 148–165. [CrossRef]

27. Kastner, M. Controls on dolomite formation. *Nature* **1984**, *311*, 410–411. [CrossRef]

28. Burns, S.J.; Baker, P.A. A geochemical study of dolomites in the Monterey Formation, California. *J. Sediment. Petrol.* **1987**, *57*, 128–129.

29. van Lith, Y.; Vasconcelos, C.; Warthmann, R.; Martins, J.C.F.; McKenzie, J.A. Bacterial sulfate reduction and salinity: Two controls on dolomite precipitation in Lagoa Vermelha and Brejo do Espinho (Brazil). *Hydrobiologia* **2002**, *485*, 35–49. [CrossRef]

30. Barkan, Y.; Paris, G.; Webb, S.M.; Adkins, J.F.; Halevy, I. Sulfur isotope fractionation between aqueous and carbonate-associated sulfate in abiotic calcite and aragonite. *Geochim. Cosmochim. Acta* **2020**, *280*, 317–339. [CrossRef]

31. Kampschulte, A.; Strauss, H. The sulfur isotopic evolution of Phanerozoic seawater based on the analysis of structurally substituted sulfate in carbonates. *Chem. Geol.* **2004**, *204*, 255–286. [CrossRef]

32. Present, T.M.; Adkins, J.F.; Fischer, W.W. Variability in sulfur isotope records of Phanerozoic seawater sulfate. *Geophys. Res. Let.* **2020**, *47*, e2020GL088766. [CrossRef]

33. Present, T.M.; Gutierrez, M.; Paris, G.; Kerans, C.; Grotzinger, J.P.; Adkins, J.F. Diagenetic controls on the isotopic composition of carbonate-associated sulphate in the Permian Capitan Reef Complex, West Texas. *Sedimentology* **2019**, *66*, 2605–2626. [CrossRef]

34. Barbiére, E.B. Condições climáticas dominantes na porção oriental da lagoa de Araruama (RJ) e suas implicações na diversidade do teor de salinidade. *Cad. Ciências Terra* **1985**, *59*, 3–35.

35. Höhn, A.; Tobschall, H.J.; Maddock, J.E.L. Biogeochemistry of a hypersaline lagoon east of Rio de Janeiro, Brazil. *Sci. Total Environ.* **1986**, *58*, 175–185. [CrossRef]

36. Moreira, I.; Patchineelam, R.; Luca Rebello, A. Preliminary investigations on the occurrence of diagenetic dolomite in surface sediments of Lagoa Vermelha, Brazil. *GeoJournal* **1987**, *14*, 357–360. [CrossRef]

37. Castro, J.W.A.; Suguio, K.; Seoane, J.; Cunha, A.M.; Dias, F.F. Sea-level fluctuations and coastal evolution in the state of Rio de Janeiro, southeastern Brazil. *An. Acad. Bras. Ciências* **2014**, *86*, 671–683. [CrossRef]

38. Seeberg-Elverfeldt, J.; Schlüter, M.; Feseker, T.; Kölling, M. Rhizon sampling of pore-waters near the sediment-water interface of aquatic systems. *Limnol. Oceanogr. Methods* **2005**, *3*, 361–371. [CrossRef]

39. Canfield, D.E.; Raiswell, R.; Westrich, J.T.; Reaves, C.M.; Berner, R.A. The use of chromium reduction in the analysis of reduced inorganic sulfur in sediments and shales. *Chem. Geol.* **1986**, *54*, 149–155. [CrossRef]

40. Rees, C.E.; Jenkins, W.J.; Monster, J. The sulphur isotopic composition of ocean water sulphate. *Geochim. Cosmochim. Acta* **1978**, *42*, 377–381. [CrossRef]

41. Böttcher, M.E.; Brumsack, H.J.; Dürselen, C.D. The isotopic composition of modern seawater sulfate: I. Coastal waters with special regard to the North Sea. *J. Mar. Syst.* **2007**, *67*, 73–82. [CrossRef]

42. Wortmann, U.G.; Chernyavsky, B.; Bernasconi, S.M.; Brunner, B.; Böttcher, M.E.; Swart, P.K. Oxygen isotope biogeochemistry of pore-water sulfate in the deep biosphere: Dominance of isotope exchange reactions with ambient water during microbial sulfate reduction (ODP Site 1130). *Geochim. Cosmochim. Acta* **2007**, *71*, 4221–4232. [CrossRef]

43. Froelich, P.N.; Klinkhammer, G.P.; Luedtke Bender, M.; Luedtke, N.A.; Heath, G.R.; Cullen, D.; Dauphin, P.; Hammond, D.; Hartman, B.; Maynard, V. Early oxidation of organic matter in pelagic sediments of the eastern equatorial Atlantic: Suboxic diagenesis. *Geochim. Cosmochim. Acta* **1979**, *43*, 1075–1090. [CrossRef]

44. Berner, R.A. A rate model for organic matter decomposition during bacterial sulfate reduction in marine sediments. *Colloq. Int. CNRS* **1980**, *293*, 35–44.

45. Lloyd, R.M. Oxygen isotope behavior in the Sulfate-Water System. *J. Geophys. Res.* **1968**, *73*, 6099–6110. [CrossRef]

46. Fritz, P.; Basharmal, G.M.; Drimmie, R.J.; Ibsen, J.; Qureshi, R.M. Oxygen isotope exchange between sulphate and water during bacterial reduction of sulphate. *Chem. Geol. Isot. Geosci.* **1989**, *79*, 99–105. [CrossRef]

47. Antler, G.; Turchyn, A.V.; Rennie, V.; Herut, B.; Sivan, O. Coupled sulfur and oxygen isotope insight into bacterial sulfate reduction in the natural environment. *Geochim. Cosmochim. Acta* **2013**, *118*, 98–117. [CrossRef]

48. Antler, G.; Turchyn, A.V.; Ono, S.; Sivan, O.; Bosak, T. Combined ^{34}S, ^{33}S and ^{18}O isotope fractionations record different intracellular steps of microbial sulfate reduction. *Geochim. Cosmochim. Acta* **2017**, *203*, 364–380. [CrossRef]

49. Jørgensen, B.B.; Findlay AJl Pellerin, A. The biogeochemical sulfur cycle of marine sediments. *Front. Microbiol.* **2019**, *10*, 849. [CrossRef] [PubMed]

50. Jørgensen, B.B.; Revsbech, N.P.; Cohen, Y. Photosynthesis and structure of benthic microbial mats: Microelectrode and SEM studies of four cyanobacterial communities. *Limnol. Oceanogr.* **1983**, *28*, 1075–1093. [CrossRef]

51. Revsbech, N.P.; Jorgensen, B.B.; Blackburn, T.H.; Cohen, Y. Microelectrode studies of the photosynthesis and O_2, H_2S, and pH profiles of a microbial mat 1. *Limnol. Oceanogr.* **1983**, *28*, 1062–1074. [CrossRef]

52. Jørgensen, B.B.; Gallardo, V.A. *Thioploca* spp.: Filamentous sulfur bacteria with nitrate vacuoles. *FEMS Microbiol. Ecol.* **1999**, *28*, 301–313. [CrossRef]

53. Jørgensen, B.B. Sulfur biogeochemical cycle of marine sediments. *Geochem. Perspect.* **2021**, *10*, 145–146. [CrossRef]

54. Brunner, B.; Bernasconi, S.M.; Kleikemper, J.; Schroth, M.H. A model for oxygen and sulfur isotope fractionation in sulfate during bacterial sulfate reduction processes. *Geochim. Cosmochim. Acta* **2005**, *69*, 4773–4785. [CrossRef]

55. Farquhar, J.; Canfield, D.E.; Masterson, A.; Bao, H.; Johnston, D. Sulfur and oxygen isotope study of sulfate reduction in experiments with natural populations from Faellestrand, Denmark. *Geochim. Cosmochim. Acta* **2008**, *72*, 2805–2821. [CrossRef]

56. Turchyn, A.V.; Brüchert, V.; Lyons, T.W.; Engel, G.S.; Balci, N.; Schrag, D.P.; Brunner, B. Kinetic oxygen isotope effects during dissimilatory sulfate reduction: A combined theoretical and experimental approach. *Geochim. Cosmochim. Acta* **2010**, *74*, 2011–2024. [CrossRef]

57. Böttcher, M.E.; Thamdrup, B.O.; Vennemann, T.W. Oxygen and sulfur isotope fractionation during anaerobic bacterial disproportionation of elemental sulfur. *Geochim. Cosmochim. Acta* **2001**, *65*, 1601–1609. [CrossRef]

58. Dole, M.; Lane, G.A.; Rudd, D.P.; Zaukelies, D.A. Isotopic composition of atmospheric oxygen and nitrogen. *Geochim. Cosmochim. Acta* **1954**, *6*, 65–78. [CrossRef]

59. Kroopnick, P.; Craig, H. Atmospheric oxygen: Isotopic composition and solubility fractionation. *Science* **1972**, *175*, 54–55. [CrossRef]

60. Mizutani, Y.; Rafter, T.A. Isotopic behaviour of sulphate oxygen in the bacterial reduction of sulphate. *Geochem. J.* **1973**, *6*, 183–191. [CrossRef]

61. Böttcher, M.E.; Smock, A.M.; Cypionka, H. Sulfur isotope fractionation during experimental precipitation of iron (II) and manganese (II) sulfide at room temperature. *Chem. Geol.* **1998**, *146*, 127–134. [CrossRef]

62. Bertran, E.; Waldeck, A.; Wing, B.A.; Halevy, I.; Leavitt, W.D.; Bradley, A.S.; Johnston, D.T. Oxygen isotope effects during microbial sulfate reduction: Applications to sediment cell abundances. *ISME J.* **2020**, *14*, 1508–1519. [CrossRef]

63. Wood, W.W.; Sanford, W.E.; Habshi, A.R.S.A. Source of solutes to the coastal sabkha of Abu Dhabi. *Geol. Soc. Am. Bull.* **2002**, *114*, 259–268. [CrossRef]
64. Vasconcelos, C.; McKenzie, J.A.; Warthmann, R.; Bernasconi, S.M. Calibration of the d^18O paleothermometer for dolomite precipitated in microbial cultures and natural environments. *Geology* **2005**, *33*, 317–320. [CrossRef]
65. Bontognali, T.R.R.; Vasconcelos, C.; Warthmann, R.J.; Bernasconi, S.M.; Dupraz, C.; Strohmenger, C.J.; Mckenzie, J.A. Dolomite formation within microbial mats in the coastal sabkha of Abu Dhabi (United Arab Emirates). *Sedimentology* **2010**, *57*, 824–844. [CrossRef]
66. Harrison, A.G.; Thode, H.G. Mechanism of the bacterial reduction of sulphate from isotope fractionation studies. *Trans. Faraday Soc.* **1958**, *54*, 84–92. [CrossRef]
67. Betts, R.H.; Voss, R.H. The kinetics of oxygen exchange between the sulfite ion and water. *Canadian J. Chem.* **1970**, *48*, 2035–2041. [CrossRef]
68. Horner, D.A.; Connick, R.E. Kinetics of oxygen exchange between the two isomers of bisulfite ion, disulfite ion ($S_2O_5^{2-}$), and water as studied by oxygen-17 nuclear magnetic resonance spectroscopy. *Inorg. Chem.* **2003**, *42*, 1884–1894. [CrossRef]
69. Kohl, I.E.; Asatryan, R.; Bao, H. No oxygen isotope exchange between water and APS–sulfate at surface temperature: Evidence from quantum chemical modeling and triple-oxygen isotope experiments. *Geochim. Cosmochim. Acta* **2012**, *95*, 106–118. [CrossRef]
70. Brunner, B.; Bernasconi, S.M. A revised isotope fractionation model for dissimilatory sulfate reduction in sulfate reducing bacteria. *Geochim. Cosmochim. Acta* **2005**, *69*, 4759–4771. [CrossRef]
71. Habicht, K.S.; Canfield, D.E. Sulfur isotope fractionation during bacterial sulfate reduction in organic-rich sediments. *Geochim. Cosmochim. Acta* **1997**, *61*, 5351–5361. [CrossRef]
72. van Lith, Y.; Warthmann, R.; Vasconcelos, C.; Mckenzie, J.A. Sulfate-reducing bacteria induce low-temperature Ca-dolomite and high Mg-calcite formation. *Geobiology* **2003**, *1*, 71–79. [CrossRef]
73. Nordeng, S.H.; Sibley, D.F. Dolomite stoichiometry and Ostwald's step rule. *Geochim. Cosmochim. Acta* **1994**, *58*, 191–196. [CrossRef]
74. Aloisi, G.; Gloter, A.; Kruger, M.; Wallmann, K.; Guyot, F.; Zuddas, P. Nucleation of calcium carbonate on bacterial nanoglobules. *Geology* **2006**, *34*, 1017–1020. [CrossRef]
75. Algeo, T.J.; Luo, G.M.; Song, H.Y.; Lyons, T.W.; Canfield, D.E. Reconstruction of secular variation in seawater sulfate concentrations. *Biogeosciences* **2015**, *12*, 2131–2151. [CrossRef]
76. Habicht, K.S.; Canfield, D.E. Isotope fractionation by sulfate-reducing natural populations and the isotopic composition of sulfide in marine sediments. *Geology* **2001**, *29*, 555–558. [CrossRef]
77. Drake, H.; Tullborg, E.L.; Whitehouse, M.; Sandberg, B.; Blomfeldt, T.; Åström, M.E. Extreme fractionation and micro-scale variation of sulphur isotopes during bacterial sulphate reduction in deep groundwater systems. *Geochim. Cosmochim. Acta* **2015**, *161*, 1–18. [CrossRef]
78. Baldermann, A.; Deditius, A.P.; Dietzel, M.; Fichtner, V.; Fischer, C.; Hippler, D.; Leis, A.; Baldermann, C.; Mavromatis, V.; Stickler, C.P.; et al. The role of bacterial sulfate reduction during dolomite precipitation: Implications from Upper Jurassic platform carbonates. *Chem. Geol.* **2015**, *412*, 1–14. [CrossRef]
79. Fichtner, V.; Strauss, H.; Immenhauser, A.; Buhl, D.; Neuser, R.D.; Niedermayr, A. Diagenesis of carbonate associated sulfate. *Chem. Geol.* **2017**, *463*, 61–75. [CrossRef]
80. Arvidson, R.S.; MacKenzie, F.T. The dolomite problem: Control of precipitation kinetics by temperature and saturation state. *Am. J. Sci.* **1999**, *299*, 257–288. [CrossRef]
81. Roberts, J.A.; Kenward, P.A.; Fowle, D.A.; Goldstein, R.H.; González, L.A.; Moore, D.S. Surface chemistry allows for abiotic precipitation of dolomite at low temperature. *Proc. Natl. Acad. Sci. USA* **2013**, *110*, 14540–14545. [CrossRef]
82. Soetaert, K.; Hofmann, A.F.; Middelburg, J.J.; Meysman, F.J.R.; Greenwood, J. The effect of biogeochemical processes on pH (reprinted from marine chemistry, Vol. 105, pp. 30–51, 2007). *Mar. Chem.* **2007**, *106*, 380–401. [CrossRef]
83. Ku, T.C.W.; Walter, L.M.; Coleman, M.L.; Blake, R.E.; Martini, A.M. Coupling between sulfur recycling and syndepositional carbonate dissolution: Evidence from oxygen and sulfur isotope composition of pore-water sulfate, South Florida Platform, USA. *Geochim. Cosmochim. Acta* **1999**, *63*, 2529–2546. [CrossRef]
84. Fike, D.A.; Grotzinger, J.P.; Pratt, L.M.; Summons, R.E. Oxidation of the Ediacaran ocean. *Nature* **2006**, *444*, 744–747. [CrossRef]
85. Gellatly, A.M.; Lyons, T.W. Trace sulfate in mid-Proterozoic carbonates and the sulfur isotope record of biospheric evolution. *Geochim. Cosmochim. Acta* **2005**, *69*, 3813–3829. [CrossRef]